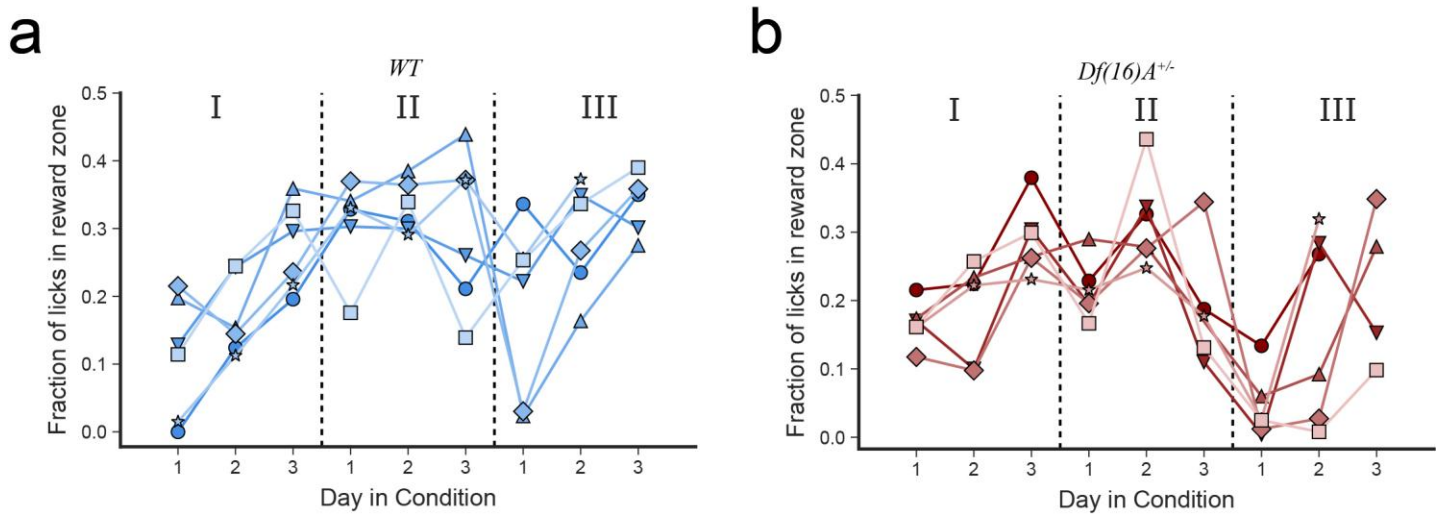

Supplementary Figure 1

Task performance by mouse

Behavioral performance per mouse across conditions of the task for (**a**) WT and (**b**) *Df(16)A*$^{+/-}$ mice. Each line is an individual mouse showing the overall task performance each day.

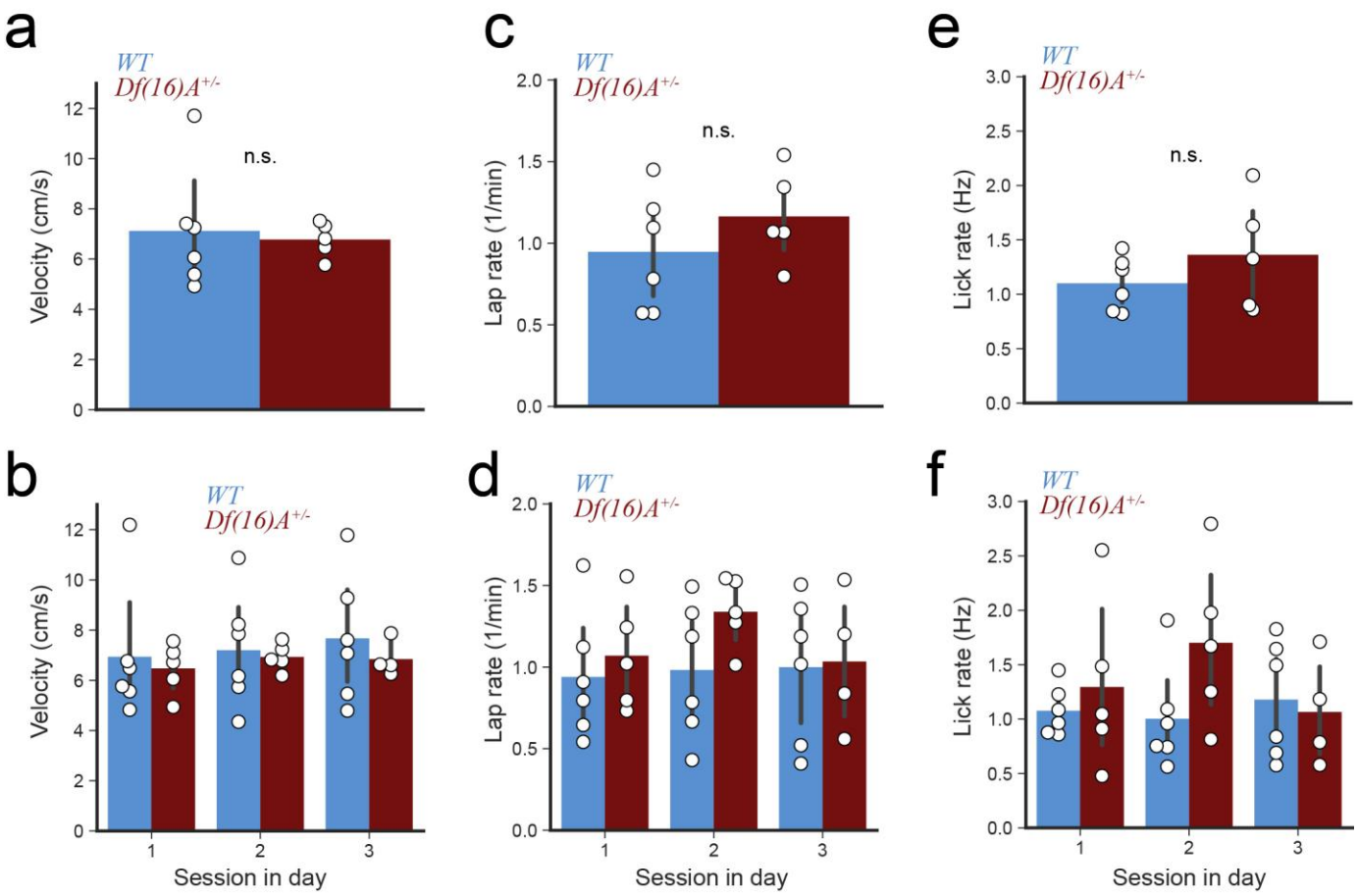

Supplementary Figure 2

Comparison of behavior during initial learning in GOL.

a. Mean velocity (excluding stationary time) during Condition I for WT and *Df(16)A*$^{+/-}$ mice. (WT: 7.123 ± 1.002, n=6 mice; *Df(16)A*$^{+/-}$: 6.778 ± 0.312, n=5 mice; independent samples T-test, t=0.302, p=0.769). **b.** Velocity during Condition I separated by session within each day (two-way ANOVA for session and genotype, all n.s.). **c,d.** Lap rate (as in *a,b*) (WT: 0.947 ± 0.147, n=6 mice; *Df(16)A*$^{+/-}$: 1.164 ± 0.128, n=5 mice; independent samples T-test, t=-1.087, p=0.305; two-way ANOVA for session and genotype, all n.s.). **e,f.** Lick rate (as in *a,b*) (WT: 1.100 ± 0.101, n=6 mice; *Df(16)A*$^{+/-}$: 1.362 ± 0.312, n=5 mice; independent samples T-test, t=-1.102, p=0.299; two-way ANOVA for session and genotype, all n.s.). Both WT and *Df(16)A*$^{+/-}$ mice show similar levels of activity during the initial learning period, as well as across sessions within each day.

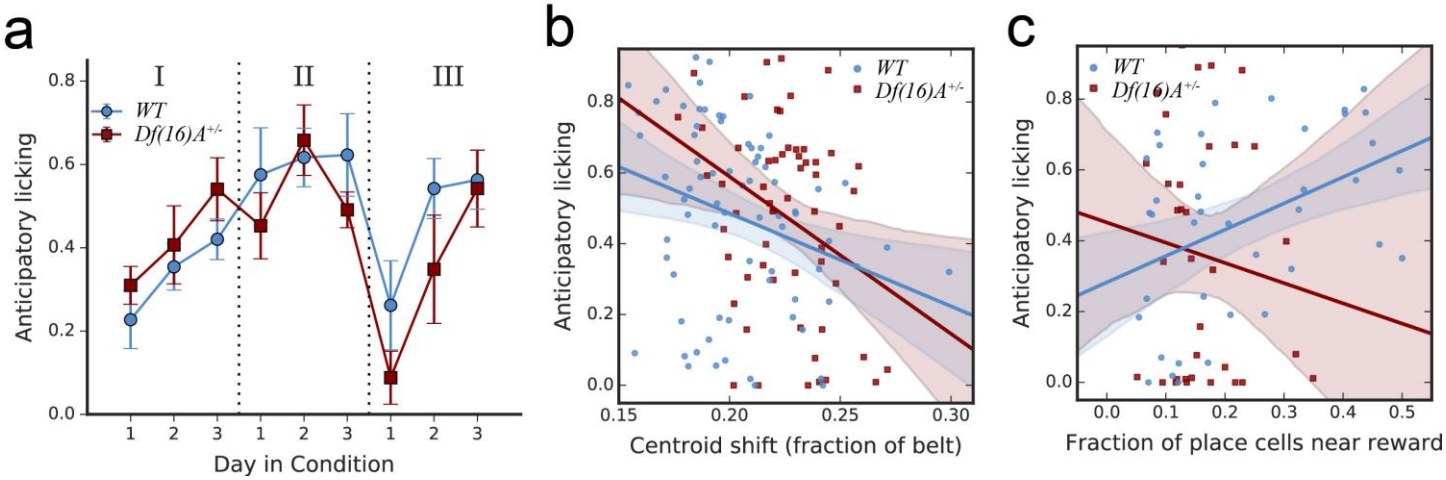

Supplementary Figure 3

Anticipatory licking

a. Task performance across all conditions of the task (Two-way mixed-effects RM ANOVA, genotype*condition interaction, p=0.060). **b.** Task performance and centroid shift correlation (centroid shift vs. fraction of licks in reward zone, Pearson's correlation coefficient, WT: -0.282, p=0.015; *Df(16)A*$^{+/-}$: -0.343, p=0.008). **c.** Task performance and goal zone place cell enrichment during Condition III (fraction of place cells near reward vs. fraction of licks in reward zone, Pearson's correlation coefficient, WT: 0.418, p=0.008; *Df(16)A*$^{+/-}$: -0.119, p=0.503).

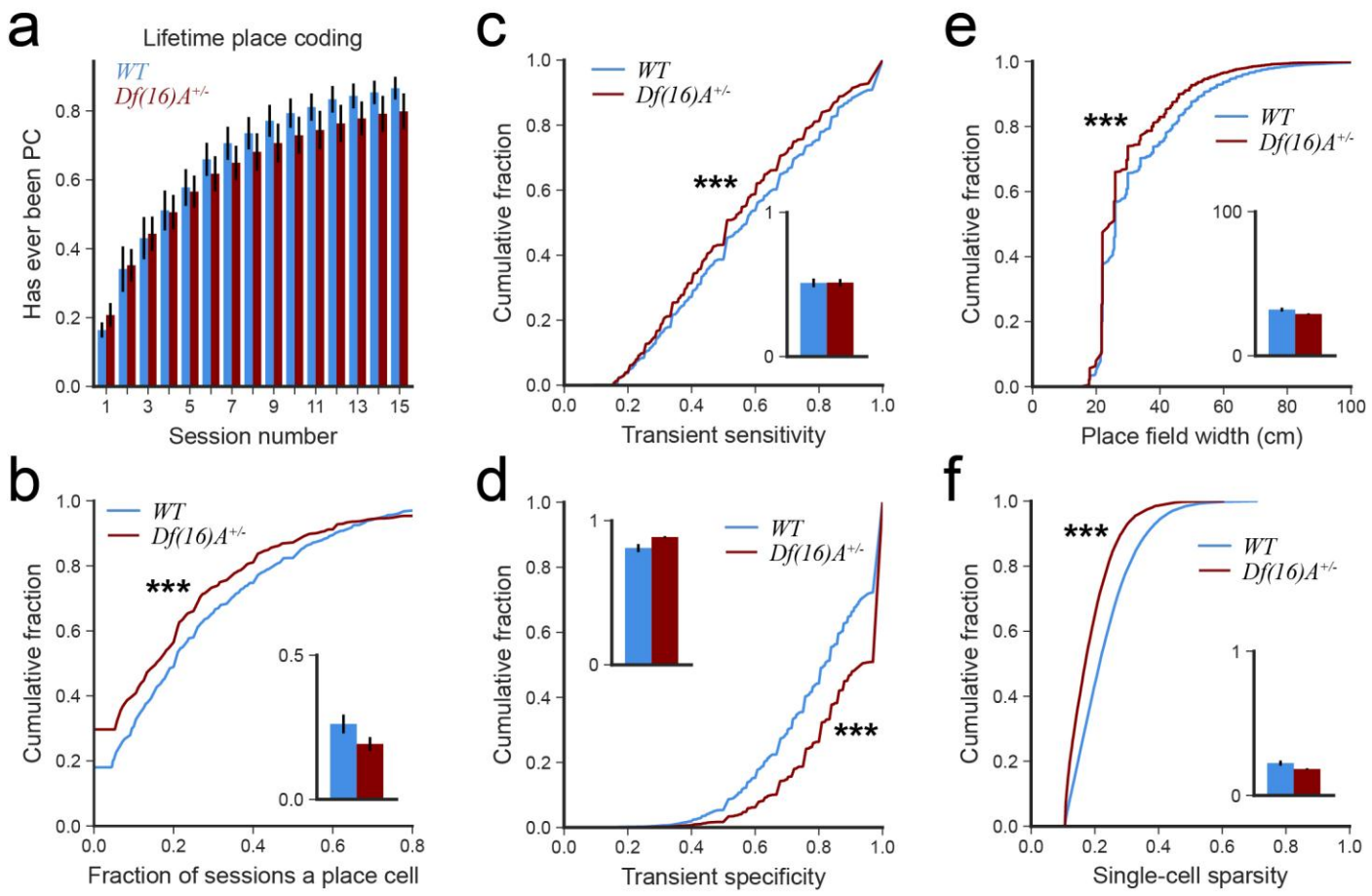

Supplementary Figure 4

Comparison of lifetime place coding and place cell metrics between *Df(16)A*$^{+/-}$ and WT mice

a. Lifetime place coding percentage, the fraction of ROIs that were ever identified as a place cell by the *n*th session imaged (lifetime place coding, Cox Regression, B=0.222, p=0.244). **b.** Fraction of all sessions imaged that an ROI was identified as a place cell (fraction of sessions a place cell; WT: 0.254 ± 0.004, n=3162 cells; *Df(16)A*$^{+/-}$: 0.214 ± 0.004, n=3322 cells; Mann-Whitney U, U=4.55x10^{6}, p<0.0001), averaged within mice (inset; independent sample T-test, t=1.517, p=0.164). **c.** Transient sensitivity, defined as the fraction of laps in which a transient occurred in the place field (WT: 0.5786 ± 0.00218, n=12524 place cell*sessions; *Df(16)A*$^{+/-}$: 0.5445 ± 0.0027, n=7664 place cell*sessions; Mann-Whitney U, U=4.4x10^{7}, p<0.0001), averaged within mice (inset, independent samples T-test, t=0.0142, p=0.989). **d.** Transient specificity, defined as the fraction of transients that occurred in the place field (WT: 0.795 ± 0.0161, n=12571 place cell*sessions; *Df(16)A*$^{+/-}$: 0.872 ± 0.0018, n=7683 place cell*sessions; Mann-Whitney U, U=3.59x10^{7}, p<0.0001), averaged within mice (inset; Welch's T-test, t=2.427, p=0.0544). **e.** Place field width (WT: 32.09 ± 0.125, n=14833 place fields; *Df(16)A*$^{+/-}$: 29.25 ± 0.136, n=8529 place fields; Mann-Whitney U, U=5.5x10^{7} p<0.0001), averaged within mice (inset, Welch's T-test, t=1.990, p=0.0911). **f.** Single-cell sparsity (WT: 0.2325 ± 0.001, n=12571 ROI*sessions; *Df(16)A*$^{+/-}$: 0.186 ± 0.001, n=8683 ROI*sessions; Mann-Whitney U, U=3.35x10^{7}, p<0.0001), averaged within mice (inset, Welch's T-test, t=2.064, p=0.0852). ***p<0.001

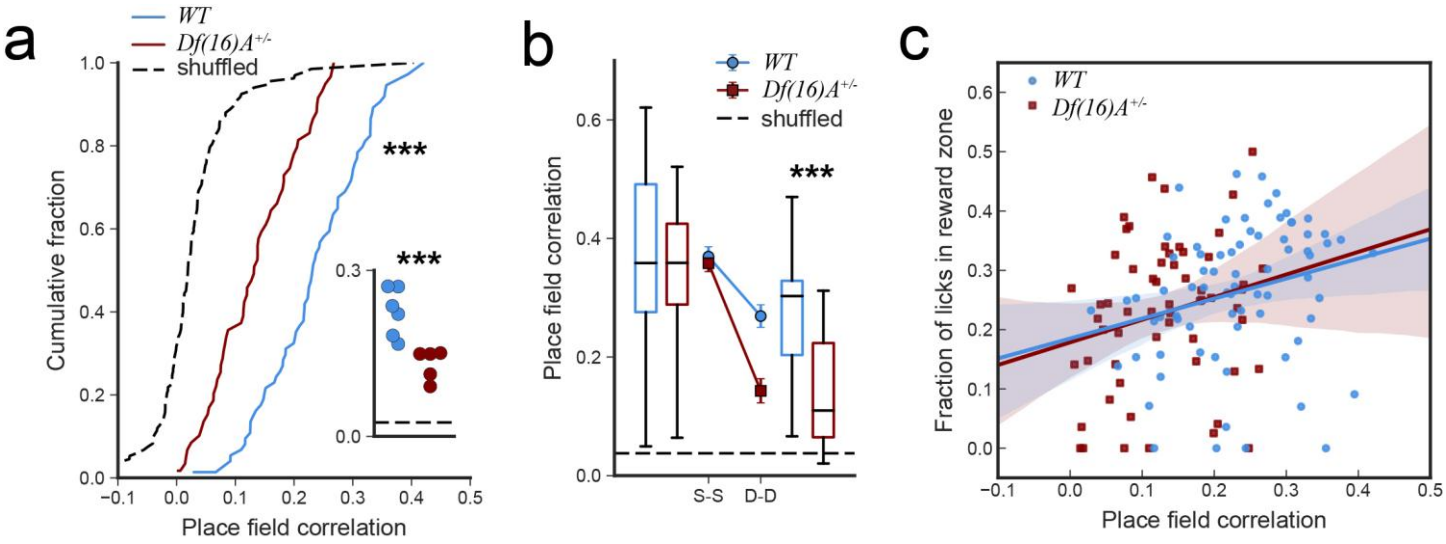

Supplementary Figure 5

Place field correlation

Place field correlation showed an overall similar effect as centroid shift (see *Fig. 3d-f*). **a.** Compared to WT mice, *Df(16)A*$^{+/-}$ mice show a significant overall decrease in place field correlation (WT: 0.232 ± 0.010, n=74 sessions; *Df(16)A*$^{+/-}$: 0.130 ± 0.010, n=59 sessions; shuffle: 0.0238 ± 0.005, n=133; WT vs. shuffle: Welch's T-test; t=18.87; p<0.0001; *Df(16)A*$^{+/-}$ vs. shuffle: Welch's T-test, t=9.89, p<0.0001; WT vs. *Df(16)A*$^{+/-}$, independent samples T-test, t=7.143, p<0.0001; inset aggregated by mouse: WT vs. *Df(16)A*$^{+/-}$: independent samples T-test, t=2.584, p=0.0295). **b.** Place fields were more stable from session-to-session than day-to-day and the *Df(16)A*$^{+/-}$ mice were less stable across elapsed time (two-way ANOVA for time elapsed and genotype, main effect of genotype: F(1,152)=5.710, p=0.0181; main effect of elapsed time: F(1,152)=55.329, p<0.0001; elapsed time*genotype interaction: F(1,152)=8.074, p=0.00511; S-S, WT vs. *Df(16)A*$^{+/-}$f: t=0.507, p=0.613; D-D, WT vs. *Df(16)A*$^{+/-}$: t=4.455; p<0.0001). **c.** Task performance correlates with the session-mean place field correlation for WT mice (Spearman's correlation coefficient=0.335, p=0.004) and trends similarly for *Df(16)A*$^{+/-}$ mice (Pearson's correlation coefficient=0.224, p=0.088).

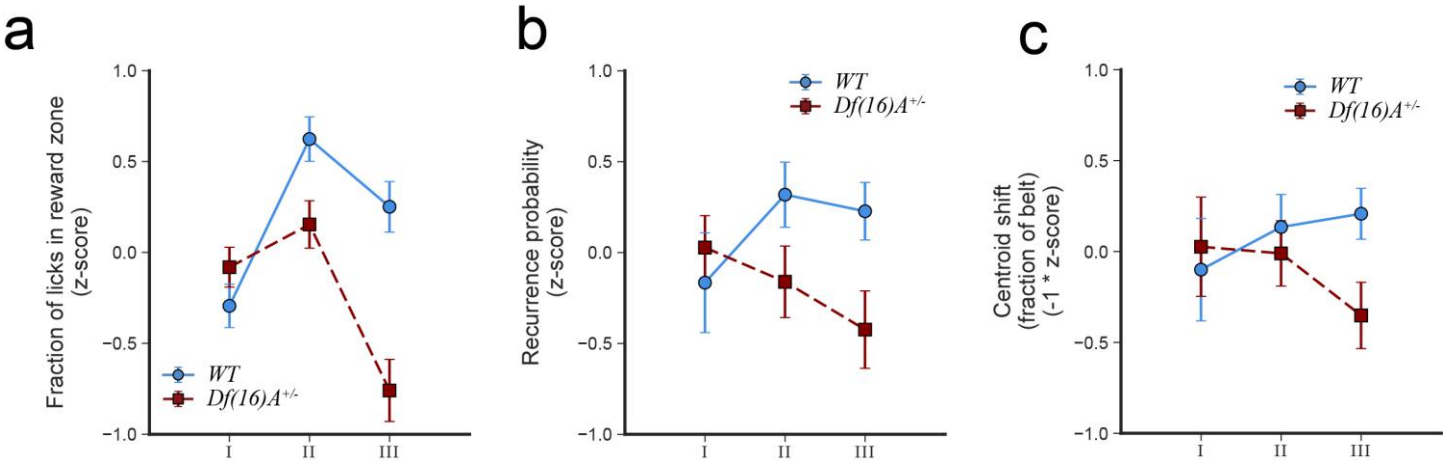

Supplementary Figure 6

Task performance, place cell recurrence, and spatial tuning stability by Condition

Task performance and population stability by genotype follows similar trajectories across conditions; that is to say, performance and stability are similar in Condition I, slightly impaired in the *Df(16)A*$^{+/-}$ mice during Condition II and most different during Condition III (three-way ANOVA, genotype*metric*condition interaction: F(4,549)=0.484, p=0.747; condition*genotype interaction: F(2,549)=11.982, p<0.0001; metric*genotype interaction: F(2,549)=0.771, p=0.463; metric*condition interaction: F(4,549)=1.503, p=0.200; Condition I, all metrics, WT vs. *Df(16)A*$^{+/-}$: independent samples T-test: t=-1.194, p=0.234; Condition II, all metrics, WT vs. *Df(16)A*$^{+/-}$: independent samples T-test: t=2.67, p=0.0081; Condition III, all metrics, WT vs. *Df(16)A*$^{+/-}$: Welch's T-test: t=5.586, p<0.0001). Same **a.** Fraction of licks in the reward zone by Condition. Same data in Fig. 3g with values transformed to z-scores (across all conditions and both genotypes). **b.** Recurrence probability by Condition. Same data in Fig. 3h with values transformed to z-scores (across all conditions and both genotypes). **c.** Mean centroid shift by Condition. Same data in Fig. 3i with values transformed to -1 * z-scores (across all conditions and both genotypes; multiplying by -1 makes positive values represent relatively increased stability). Bonferroni-corrected post hoc tests comparing genotype per condition; *p<0.05, **p<0.01, ***p<0.0001.

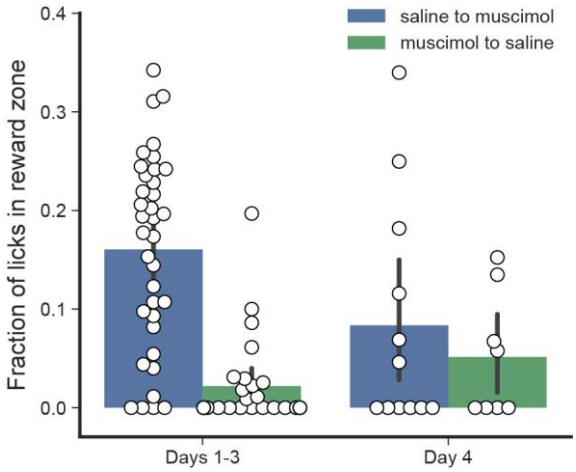

Supplementary Figure 7

Impaired task performance during CA1 inactivation.

During initial learning of a reward location, local inactivation of CA1 lead to significantly reduced task performance (Days 1-3, muscimol to saline vs. saline to muscimol: Mann-Whitney U, U=126.5, $p<0.0001$). In addition, mice which received saline infusion during the first three initial learning days performed significantly worse on the fourth day when they were infused with muscimol (saline to muscimol, Days 1-3: 0.221 ± 0.053, n=36 sessions; Day 4: 0.084 ± 0.034, n=12 sessions; Mann-Whitney U, U=111, $p=0.0235$) and now performed at a similar level to mice which were initially infused with muscimol (Day 4, saline to muscimol vs. muscimol to saline: independent samples T-test, $t=0.633$, $p=0.535$).

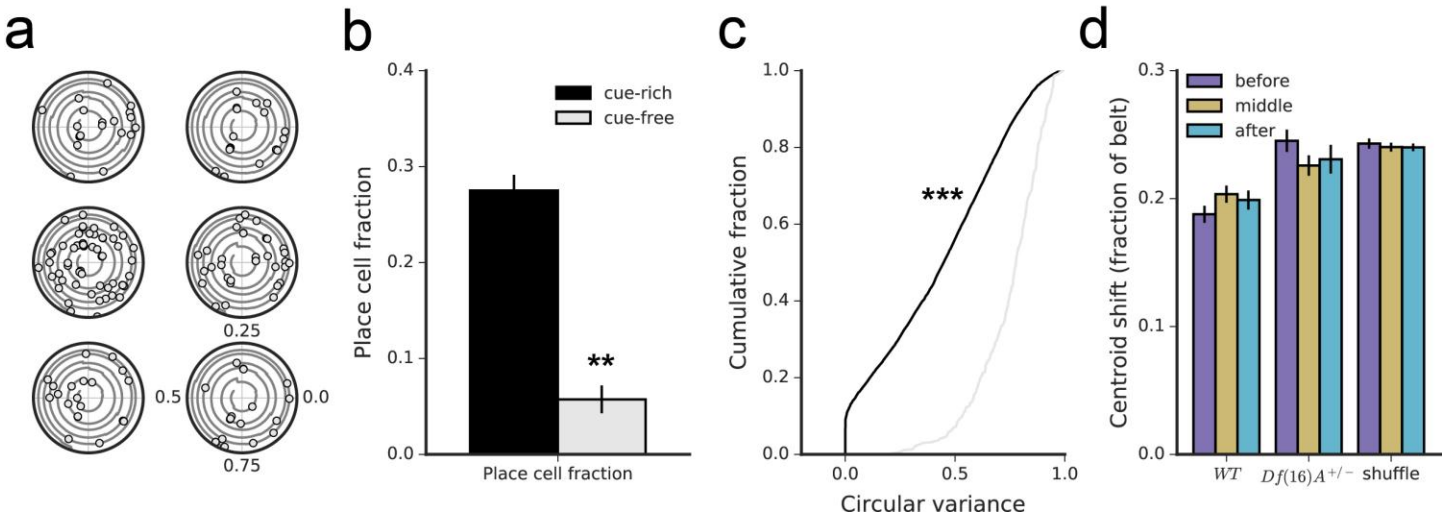

Supplementary Figure 8

No place cells on a cue-free belt; spatial tuning near the fabric-transition is not more stable

a. The 6 most spatially-tuned cells (lowest circular variance) on a burlap belt, plotted as in Fig. 2c. **b.** Place cell fraction on a 'cue-rich' and 'cue-free' belt during RF (cue-rich: 0.275 ± 0.017, n=56 sessions; cue-free: 0.057 ± 0.018, n=3 sessions; independent samples T-test, t=3.006, p=0.004). **c.** Transient circular variance on a 'cue-rich' and 'cue-free belt during RF (cue-rich: 0.427 ± 0.003, n=7828 cell*sessions; cue-free: 0.746 ± 0.008, n=375 cell*sessions; Mann-Whitney U, U=4.99x10^5, p<0.0001). **d.** Centroid shift of cells from the last day of Condition I to the first session of Condition II separated by tuning preference relative to fabric transitions—the only features that remain constant between the two contexts. WT tuning is generally more stable (WT vs. *Df(16)A*$^{+/-}$, independent samples T-test: t=-4.96, p<0.0001; see *Fig. 4a*), but neither genotype shows increased stability near the fabric transitions (two-way ANOVA, main effect of binned distance: F(2,24)=0.024, p=0.977). **p<0.01, ***p<0.001

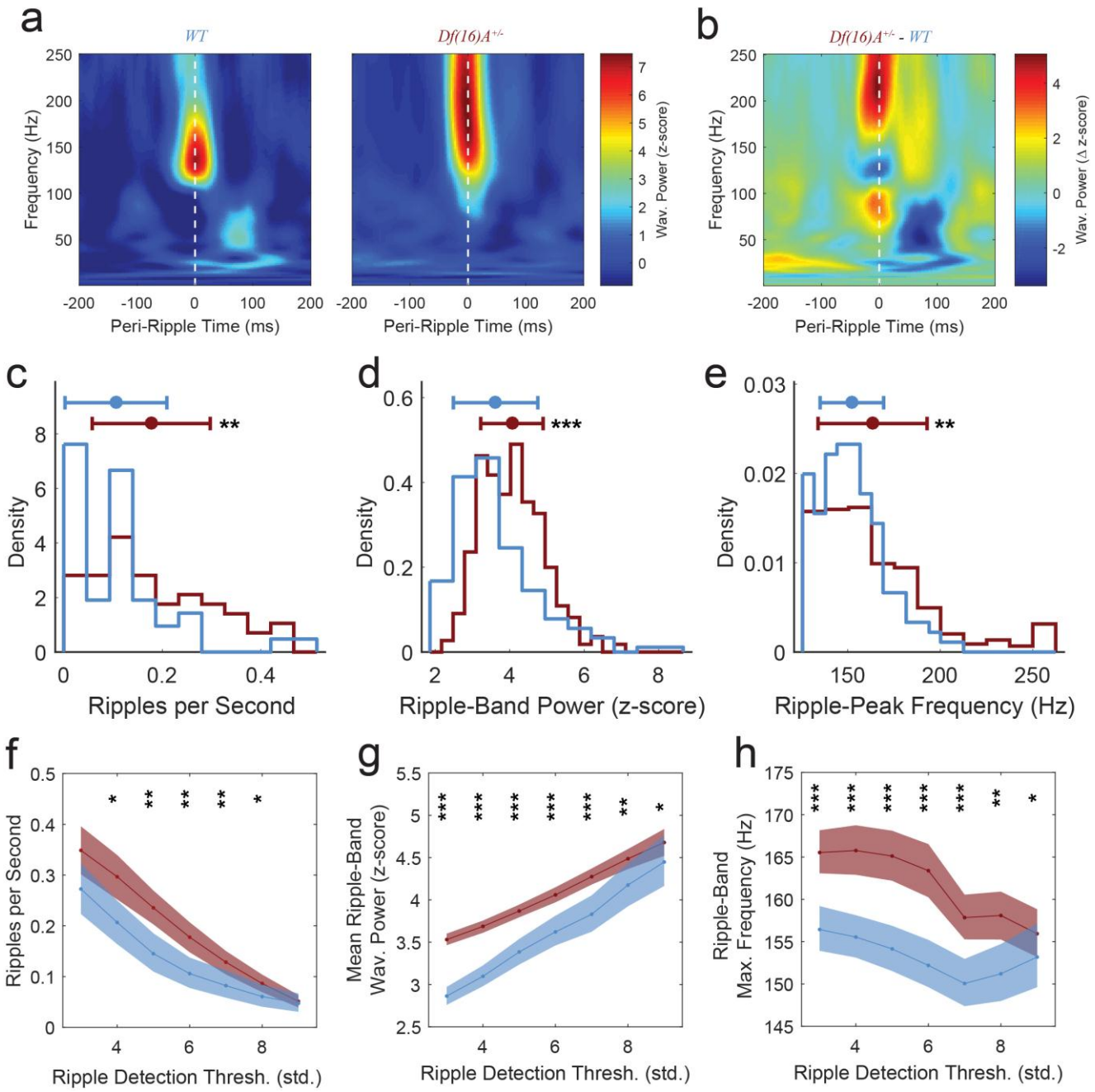

Supplementary Figure 9

Sharp wave-ripples (SWR) are altered in *Df(16)A*$^{+/-}$ mice

a. Mean SWR wavelet power for WT (left) and *Df(16)A*$^{+/-}$ (right) mice. **b.** Difference (*Df(16)A*$^{+/-}$ - WT) of mean SWR wavelet power in *a.* **c.** Rate of SWRs during stationary bouts (mean ± SD; WT: 0.106 ± 0.103, n=45 stationary intervals; *Df(16)A*$^{+/-}$: 0.178 ± 0.120, n=61 stationary intervals; Wilcoxon rank-sum test, h=3777.5, p=0.00096). **d.** Mean wavelet power (mean ± SD; WT: 3.622 ± 1.133, n=145 sharp wave-ripples; *Df(16)A*$^{+/-}$: 4.060 ± 0.838, n=357 sharp wave-ripples; Wilcoxon rank-sum test, h=98423, p<0.0001). **e.** Frequency with maximum power (mean ± SD; WT: 152.190 ± 17.174, n=145 sharp wave-ripples; *Df(16)A*$^{+/-}$: 163.391 ± 29.485, n=357 sharp wave-ripples; Wilcoxon rank-sum test, h=94798, p=0.00066). **f-h.** Same as (*c-e*) for several SWR detection thresholds (significance by Wilcoxon rank-sum test as marked). *p<0.05, **p<0.001, ***p<0.0001. SWR-related place cell reactivation (for example, as in Wilson and McNaughton, Science, 1994; Lee and Wilson, Neuron, 2002; Foster and Wilson, Nature 2006) was not directly assessed.

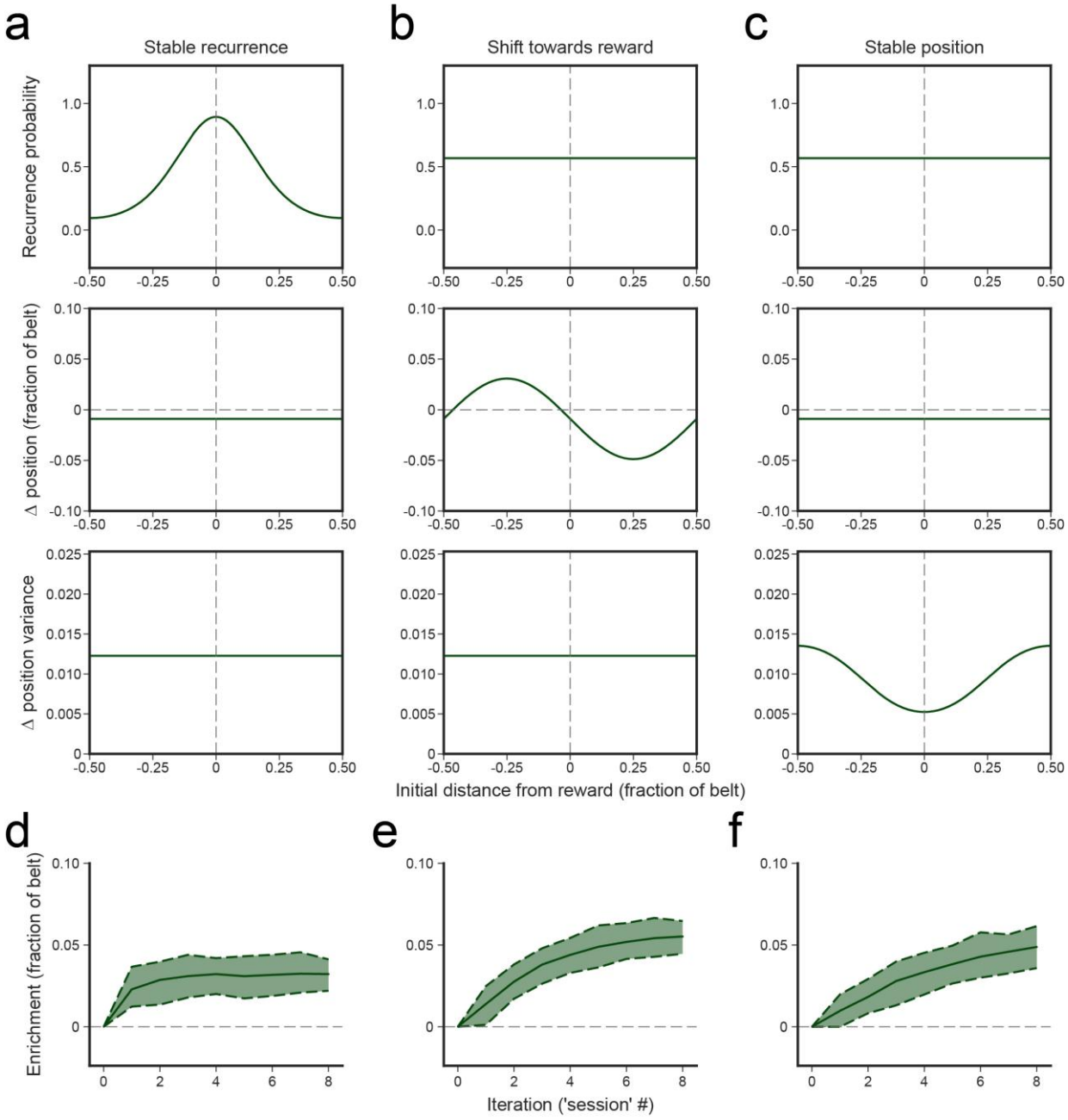

Supplementary Figure 10

Possible enrichment mechanisms

Comparison of three theoretical methods by which place cells could enrich a goal location. **a.** Place fields could be generally stable, but place cells near the reward are more likely to reoccur as place cells from session-to-session. (top) Recurrence probability as a function of distance from reward. (middle) Mean place field centroid shift as a function of distance from reward. (bottom) Mean place field shift variance as a function of distance from reward. **b.** Place cells could reoccur at equal probability along the belt, but place fields shift towards the reward location such that fields before the reward shift forward and fields after the reward shift backwards. Plots as in *a*. Place fields shifting towards the reward also leads to enrichment in our model. **c.** Place fields might not shift uniformly towards the reward, but if fields are generally stable, the ones near the reward could shift less than ones farther away. Plots as in *a*. **d-f.** Using the parameters from *a-c*, our enrichment model suggests all three hypothetical models could lead to enrichments: (**d**) increased place cell recurrence at reward position, (**e**) place fields shifting towards the reward location, or (**f**) place fields near the reward shifting less than ones away from the reward.

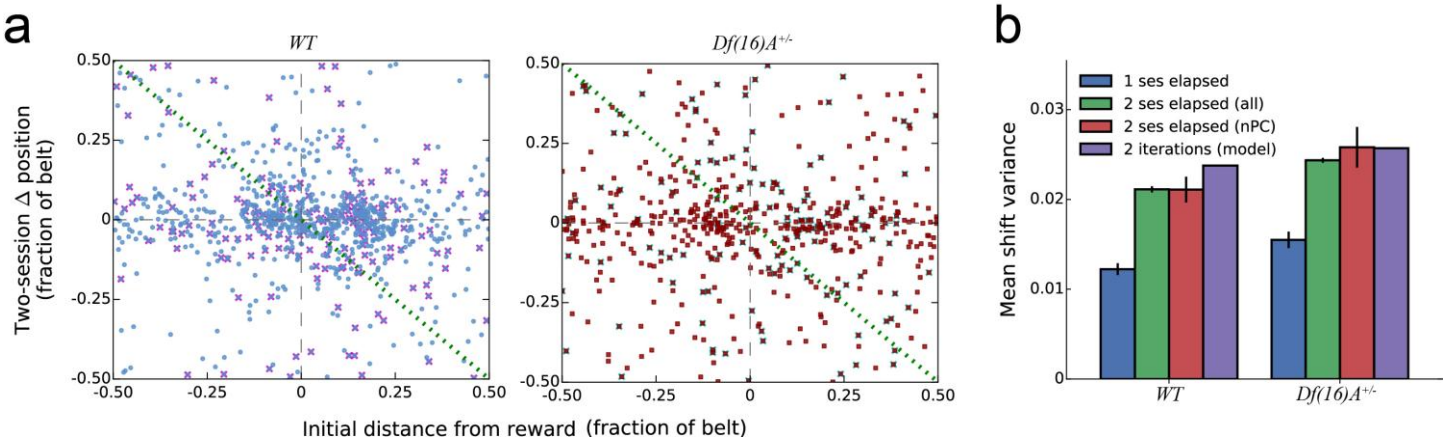

Supplementary Figure 11

Latent spatial tuning revealed across multiple sessions

a. Scatter plots of original position versus position shift after 2 elapsed sessions for WT and *Df(16)A*$^{+/-}$ mice. Cells that were not a place cell in the middle session are marked in magenta and cyan for WT and *Df(16)A*$^{+/-}$ data, respectively. Even cells that were not a place cell in the intervening session still cluster around 0, suggesting that they retain some latent place preference that is either not expressed or not detectable. Vertical dashed line denotes reward location. Horizontal dashed line marks fields that do not shift at all. Green diagonal dashed line marks fields that remap directly to the reward location. **b.** Mean place field shift variance across all positions for cells paired by 1 session elapsed, 2 sessions elapsed, 2 sessions elapsed for cells that were not a place cell in the intervening session, and 2 iterations of the model. Two-session elapsed place cells are equally stable whether or not the cell was a place cell in the middle session, which is also the same as two iterations of the model.

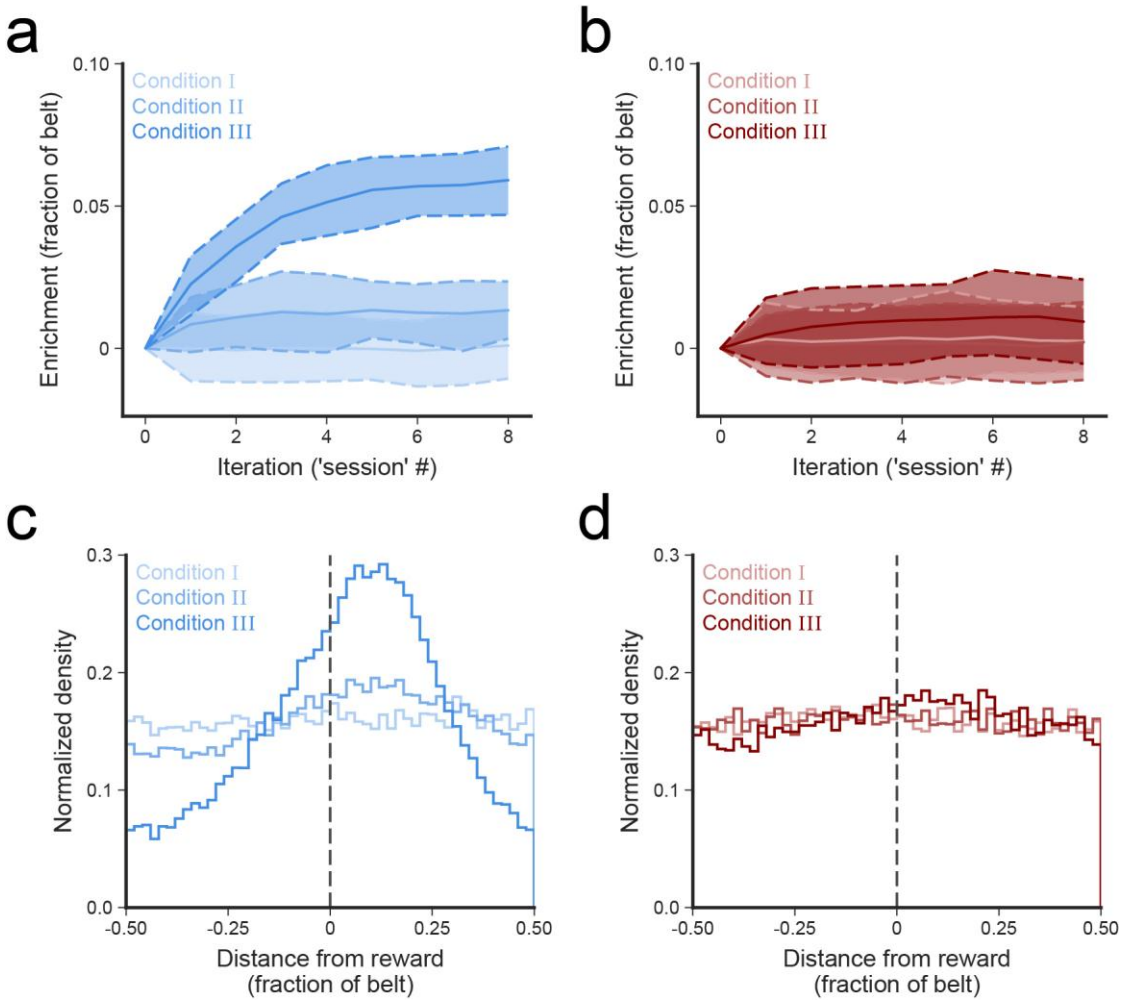

Supplementary Figure 12

Modeled enrichment for all three Conditions

Our model of place cell enrichment only produces goal location enrichment with parameters fit from WT mice during Condition III. **a,b.** Enrichment by iteration with parameters fit from each of the three Conditions of the task for (*a*) WT and (*b*) *Df(16)A*$^{+/-}$ mice (as in *Fig. 7b, 8e*). **c,d.** Final distribution of place fields after 8 iterations for each set of parameters fit from (*c*) WT and (*d*) *Df(16)A*$^{+/-}$ mice (as in *Fig. 7c, 8f*).

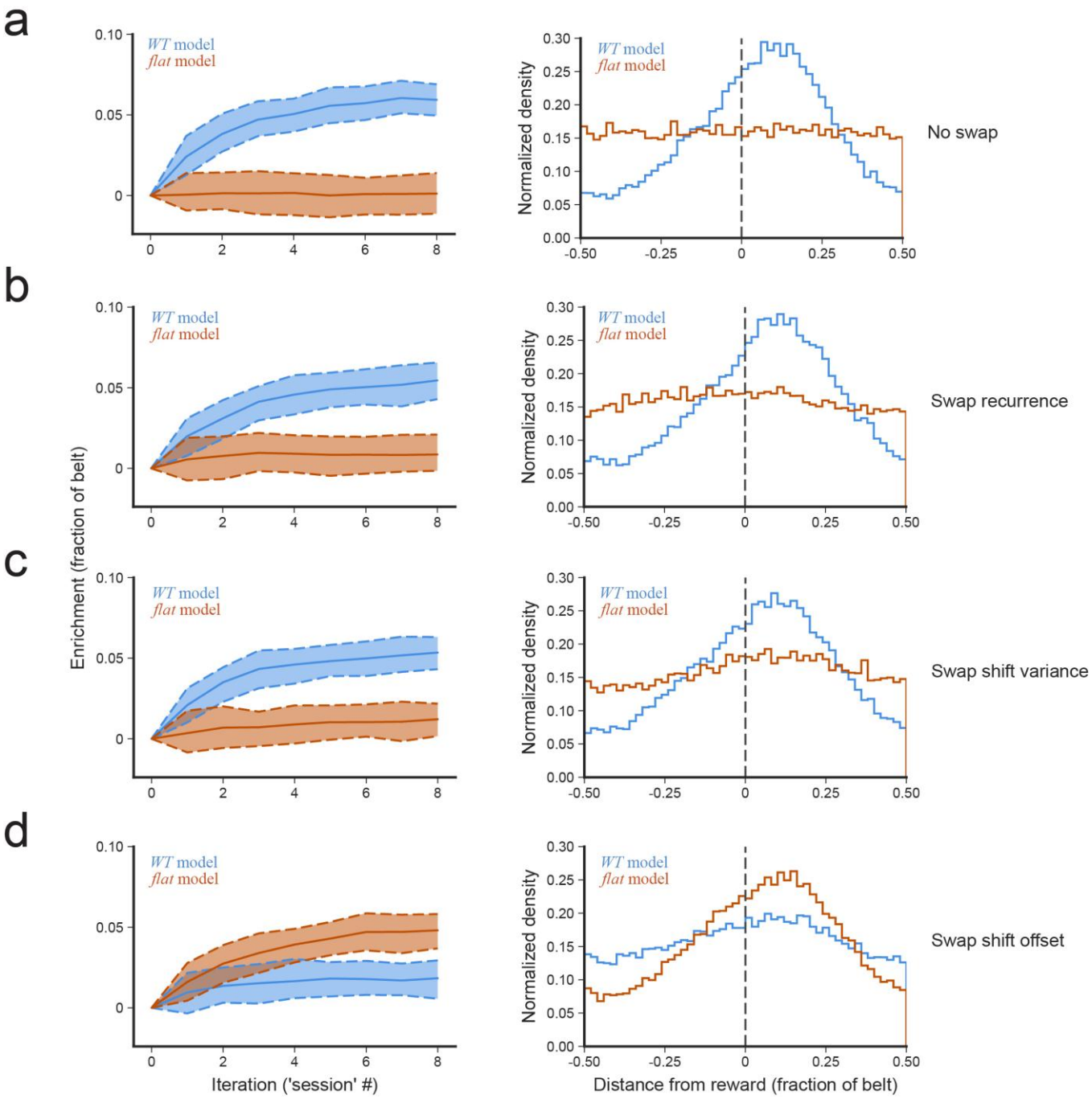

Supplementary Figure 13

Model enrichment when swapping individual parameters between WT and *Df(16)A*$^{+/-}$ values

Mean enrichment by iteration (left, 90% confidence interval shading determined from 100 simulations) and histogram of distributions of place fields after the final iteration (right, data pooled across all simulations, vertical dashed line denotes reward location) for each parameter individually swapped between WT and *flat* models. **a.** No swap. **b.** Swap place cell recurrence probability (P_{recur}). **c.** Swap session-to-session place field shift variance. **d.** Swap session-to-session place field shift offset. Swapping shift offset has the largest effect, as the *flat* model with only the WT shift offset parameters leads to enrichment, while the WT model with the *flat* shift offset parameters does not.